CuTi2S4/REDUCED GRAPHENE OXIDE ASSISTED PHOTOCATALYTIC DEGRADATION OF REACTIVE BLACK-5

Priya Perumal[1], Lakshmi mahadevan[2*]

Article History: Received: 04.06.2023 **Revised:** 04.07.2023 **Accepted:** 01.08.2023

Abstract

Photocatalytic degradation is one of the most attractive, low-cost and sustainable technologies for removing pollutants from waste water. Especially dual metal sulfide-combined graphene-based materials are excellent photocatalysts due to their faster electron transfer ability. Herein, we developed copper titanium sulfide ($CuTi_2S_4$) composite-anchored reduced graphene oxide (rGO, $CuTi_2S_4$/rGO) material by a feasible hydrothermal approach. The prepared $CuTi_2S_4$/rGO material was employed for a degradation of reactive black-5 (RB-5). During the synthesis process, the conversion of graphene oxide into reduced graphene oxide is followed by the in situ deposition of Cu, Ti and S precursors. The resultant material can significantly promote the interfacial contact between $CuTi_2S_4$ and rGO, leading to the formation of an active $CuTi_2S_4$/rGO composite material. The highly effective anchoring of $CuTi_2S_4$ over the rGO material facilitates the transfer of photogenerated electrons from $CuTi_2S_4$ to rGO, altering the photocatalytic degradation of RB-5 efficiency under visible light irradiation. In addition, $CuTi_2S_4$/rGO reveals a higher photocatalytic response with a band gap of 1.8 eV, which is mainly attributed to the higher adsorption and desorption sites and the excellent charge carrier ability between rGO and $CuTi_2S_4$ composite. These studies provide excellent strategies for developing highly stable and effective rGO-based catalyst materials for purifying pollutants and their related applications.

Keywords: Photocatalyst, $Cuti_2S_4$, Reduced Graphene Oxide, Hydrothermal Approach, Reactive Black-5.

[1]Department of Chemistry, Periyar University, Salem-636 011, Tamil Nadu, India.
[2*]Department of Chemistry, Namakkal Kavignar Ramalingam Government Arts College for Women, Namakkal-637 001, Tamil Nadu, India.

Email: [2*]drmlakshmichemap@gmail.com

[*]Corresponding Author:
Lakshmi Mahadevan[2*]
[2*]Department of Chemistry, Namakkal Kavignar Ramalingam Government Arts College for Women, Namakkal-637 001, Tamil Nadu, India.
Email: [2*]drmlakshmichemap@gmail.com

DOI: 10.31838/ecb/2023.12.s3.789

1. Introduction

Due to the growing population and the usage of various products, huge environmental issues have arisen, especially organic pollution which is generated from cosmetics, textiles, and various industries [1–4]. Particularly, the industrial waste contains various traces of metal ions such as Cr, Cd, Hg, As, and various organic pollutants [5]. Especially the hexavalent of Cr has a huge toxic nature and is also a non-biodegradable pollutant, which creates enormous health issues such as liver damage and cancer. At the same time, it releases the one of the major organic pollutants of phenolic compounds, which also has impacts on human health. So it is best to remove it before putting it into the running water. These pollutants can be detached by various physical, chemical and biological methods like precipitation, adsorption, reverse osmosis, ozonization, ultrafiltration, and flocculation [6].

Among the various methods, photodegradation is of superior interest and an excellent treatment for removing toxic chemicals and pollutants [4]. As a result, various studies have focused on the photocatalytic approach for the removal of epidemics. In recent years, metal chalcogenide materials have become more attractive and suitable candidates for various applications, including optoelectronics and energy storage, as well as biomedical applications [7–11]. Due to its higher conductivity which significantly improves multiple application performance compared to that of metal oxides. Among the various types of chalcogenides, CuS has great potential in the fields of catalysis and photovoltaics [12]. In one of the reports, Krishnamoorthy et al. prepared the CuS nanoparticles using a one-step hydrothermal approach. The resultant yield of the covalent phase of cubic-shaped CuS nanoparticles demonstrated a higher pseudo-capacitor nature [13]. In addition, Saranya et al. reported that the various morphologies of CuS nanostructures were prepared by the hydrothermal treatment with the aid of copper chloride, thiourea, and thiosulpahte precursors. They proved that the obtained CuS hexagonal phase and their urchin and nanoplate morphologies significantly improved the optical properties with a band gap of 2.12 and 2.18 eV [14]. Notably, the co-precipitation yield of the CuS nanoparticles richest has the highest electrical conductivity of 72.9 S/cm at 55 ^oC, as reported by Ramalingam et al [15]. Similarly, Bejjai et al. also utilised a similar method for the preparation of CuS, altering the Cu forerunners such as $CuCl_2$, CuCl, and $CuSO_4$ combined with thiourea (S source) and fixing their molar ratio. They demonstrated that the type of Cu source and the Cu/S molar ratios are mainly responsible for varying the band gap from 2.05 to 2.34 eV and improving the absorbance of visible light [16]. However, the single compounds along with the low separation efficiency of photogenerated charge carriers, are very essential for large-scale application studies.

In addition, graphene oxide (GO) is proven to be the most adopted material for the degradation of dyes owing to its impressive properties, such as its large surface area, higher functional groups, attractive band structure, higher mechanical strength and higher conductivity [4]. In this regard, great attention was focused on the graphene metal oxide composite, which altered the concentrations and their ratios. In this regard, recently, Muthukrishnaraj et al. developed a graphene-incorporated Cu_2O composite by the precipitation method. They established that the 2 wt% incorporated Cu_2O composite exhibited remarkable degradation efficiency for methylene blue (97.9%) and methylene orange (96.1%) [4]**.** Further, Arumugam et al. synthesised the photocatalytic material of NiS and reduced graphene oxide (rGO) through the hydrothermal approach by utilising nickel chloride hexahydrate and sodium sulfide hydrate sources. They attested that the obtained NiS/rGO revealed a greater photocatalytic degradation activity against methylene blue, and its removal percentage reached 87% [17]. Dutta et al. claimed that the ZnS/rGO composite delivered a higher photocatalytic activity (99.9%) than that of hollow ball-shaped ZnS (degradation activity, 97.14%). They mentioned that the higher surface area and the better charge carrier transportation are the main reasons for improved photocatalytic acitivity [18].

On the other hand, CuS/rGO composites are also excellent materials, and they are considered suitable materials for the application of photodegradation of organic pollutants [19,20]. Cherifi et al. developed the CuS/rGO composite with different width ratios through the hydrothermal approach and achieved remarkable photocatalytic activity under visible light irradiation [21]. In addition, $CuCo_2S_4$/RGO composites delivered admirable photocatalytic degradation for the malachite green pollutant. The 3% rGO in $CuCo_2S_4$ and its synergistic effect are highly beneficial for improved performance, as was testified by Vadivel and co-workers [22]. Consequently, Cu_2SnS_3/rGO, with flower-shaped morphologies derived from thiourea and polyvinylpyrrolidone sources, exhibited notable photocatalytic performance for the degradation of Rhodamine B [23]. Similarly, Ca/$ZnIn_2S_4$ and $CuCo_2S_4$ materials combined with rGO also effectively improved the photocatalytic performance [22,24,25]. Recently, we prepared the $CuZr_2S_4$ doped with rGO composite by employing copper nitrate, zirconium oxy nitrate, and metallic sulfur. The as-prepared $CuZr_2S_4$/rGO material significantly promoted the M-O-M moieties and the nanoflower-like morphology, which resulted in enhanced photocatalytic performance [26].

Inspired by these strategies, we have developed a bimetallic sulfide ($CuTi_2S_4$) of reduced graphene oxide composite by a single-step hydrothermal process. The introduction of copper nitrate, tetraethoxy titanium (tetraethyl ortho titanate), and metallic sulfur in reduced graphene oxide significantly influences functional groups and their morphologies. Subsequently, the resulted $CuTi_2S_4$/rGO material displayed the cubic crystal structure and $CuTi_2S_4$ combined stable sheet-like morphologies, and the higher Cu, Ti, and S contents in rGO greatly modified the photocatalytic activity of reactive black-5 dye removing process. The higher photocatalyttic performance can be ascribed to the higher absorption and desorption abilities along with the excellent charge carrier capability between rGO and $CuTi_2S_4$ composite. To the best of our knowledge, this is the first report on the utilisation of the above-mentioned precursors for developing a highly ordered sheet like $CuTi_2S_4$/rGO composite using phtocatalytic studies of the reactive black-5 degradation.

2. Experimental section

2.1 Chemicals and reagents

Copper nitrate ($Cu(NO_3)_2.3H_2O$) were obtained from the SRL. Ethanol (CH_3OH), sodium nitrate ($NaNO_3$), reactive black-5, dimethyleneamine and the metallic sulfur were procured from Alfa Aeaser. Sodium hydroxide (NaOH) was purchased from Merck. Tetraethoxy titanium (tetraethyl orthotitanate, $Ti_4(OCH_2CH_3)_{16}$) was purchased from Sigma Aldrich.

2.2 Synthesis of pure $CuTi_2S_4$ and rGO combined $CuTi_2S_4$ nanocomposite

A single step preparation of reduced graphene oxide based on our previously reported method [26]. The synthesis process of $CuTi_2S_4$ composite was done by a hydrothermal approach in a one-step process. Initially, 3 mM of copper nitrate was mixed in ethanol (30 mL) and the obtained mixture was added dropwise to 3 mM of tetraethoxytitanium (Ti precursor) and 3 mM of sulfur solution under magnetic stirring for 2 h. Consequently, the obtained composites was transferred into an autoclave and heated at 140 ^oC for 8 h. Finally, the precipitate was filtered, washed with ethanol and dried to produce the $CuTi_2S_4$ composite material.

The synthesis of $CuTi_2S_4$/rGO nanocomposite was performed as follows: 250 mg of prepared $CuTi_2S_4$ material was mixed with 30 mL of ethanol solution and continuously stirred for 2 h. Consequently, the above mixture was blended with 150 mg of rGO solution. Then the attained mixture was transferred to an autoclave and kept in a hot air oven at 140 ^oC for 8 h. Finally obtained precipitate was washed several times with ethanol labelled as $CuTi_2S_4$/rGO.

2.3 Characterization

The structures of the pure $CuTi_2S_4$ and rGO combined materials were inspected by an X-ray diffractometer (XRD) Rigaku with a scan rate of 3^o/min and recorded a 2 theta range of

10 to 90°. Then, Raman spectra from a model of LabRAM HR evolution (Horiba) with a wavelength of 532 nm was used to confirm the formation of the $CuTi_2S_4$/rGO structure. The morphologies and elemental percentages of prepared $CuTi_2S_4$/rGO were examined by field emission scanning electron microscopy (FESEM), ZEISS (EVO LS 15, Germany) instrument and elemental dispersive X-ray (EDX) analysis was performed with the help of AMETEK, Z2-17 analyzer (USA). Further, the insight morphology and their crystalline nature analyses were carried out by high resolution transmission electron microscopy (HRTEM, FEI). Fourier transform infrared spectra with a model of Bruker Optic, Gmbh, Germany (TENSOR 27) were used to evaluate the bonding site of $CuTi_2S_4$/rGO materials.

2.4 Evaluation of photocatalytic performance

A photocatalytic study was carried out using a homemade photocatalytic reactor system using organic reactive dye under UV-Visible radiation and illuminated by a tungsten halogen lamp (500 W). Then the reactor temperature was controlled by a continuous flow of water in its outlet. Then, 100 mL of 20 ppm dye solution containing 50 mg nanocomposite catalysts employed as the photocatalyst in the photoreactor. Continuously, after switching on the lamp, the resultant concentration of dye was measured with the help of an Elico UV-Vis spectrophotometer. Afterward, the effect of oxidants was estimated in a similar way with the addition of measured quantities of oxidant solution (1 M) to the dye solution.

The percentages of degradation was estimated as $\frac{C_o - C}{C_o} \times 100$

Here Co and C are the initial concentration and the concentration of the dye after degradation, respectively.

In addition, the degradation analysis was carried out by Langmuir-Hinshelwood kinetic model and its formulas as follows

$$R_s = \frac{kKc}{1 + KC}$$

Here, r_s and C are the specific degradation reaction rate (mg/min) and the concentration of the dye (mg), respectively. The k and K are the reaction rate constant (min) and the dye adsorption constant. Besides, the C is small, the above mentioned equation and obtained apparent pseudo first-order equation is

$$R_s = kKC = K_{app}\, C \left(= -\frac{dc}{dt}\right)$$

$$-\ln\left(\frac{C}{Co}\right) = k_{app}\, t$$

3. Result and Discussion

3.1 $CuTi_2S_4$/rGO material structure and characterization

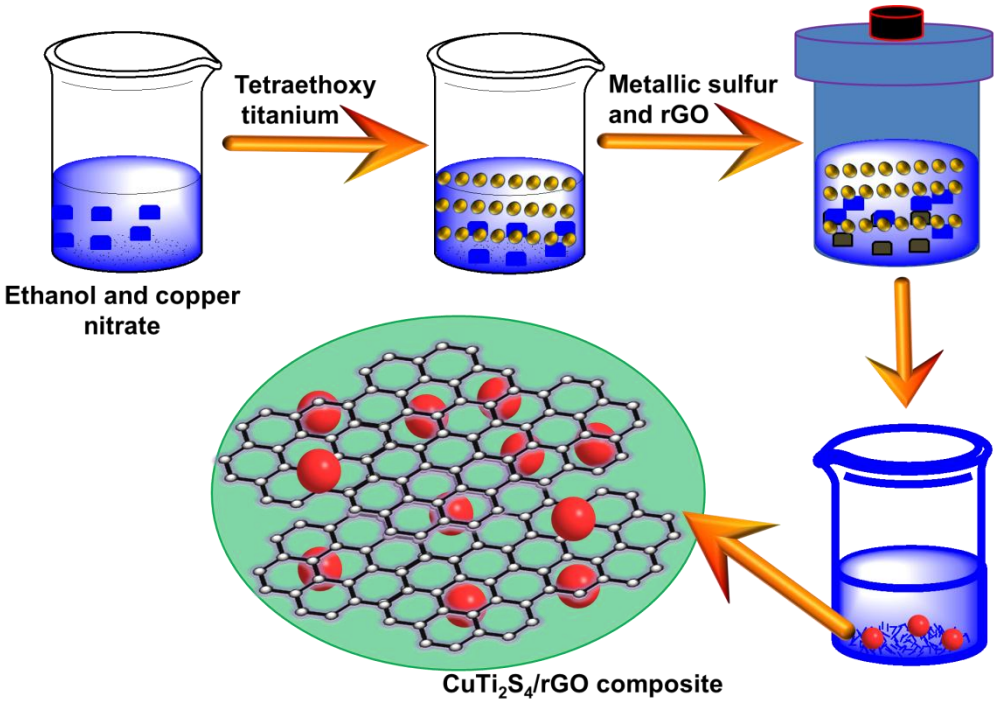

Scheme 1. Schematic representation of the preparation of $CuTi_2S_4$/rGO composite by hydrothermal process.

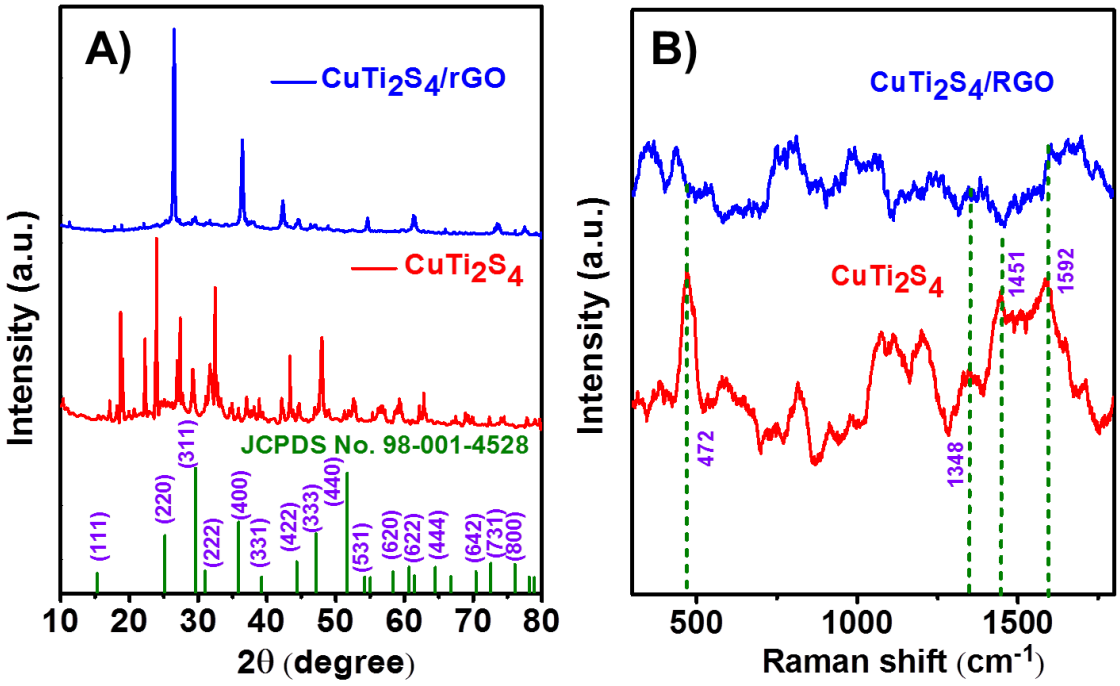

Figure 1. (A) XRD pattern and Raman spectra of prepared the $CuTi_2S_4$/rGO and pure $CuTi_2S_4$ materials.

Scheme 1 illustrates the schematic preparation of the $CuTi_2S_4$/rGO composite material. Initially, copper nitrate was dissolved in ethanol and then titanium precursor of tetraethoxytitanium was added under constant stirring. Then the addition of metallic sulfur was combined with Cu and Ti precursors to promote a $CuTi_2S_4$ under a hydrothermal process. Afterward, the $CuTi_2S_4$ was mixed with the rGO solution. The resulting product

was transformed into a $CuTi_2S_4$-anchored rGO composite during the hydrothermal treatment. **Figure 1A**. the XRD pattern, the main peaks are at 15.3, 25.1, 29.6, 30.9, 35.8, 39.2, 44.3, 47.1, 51.6, 54.2, 58.3, 61.4, 64.5, 70.4, 72.5 and 76.0°, which are indexed to (111), (220), (311), (222), (400), (331), (422), (333), (440), (531), (620), (622), (444), (642), (731) and (800) planes, respectively. Such observations are well matched with JCPDS:98-001-4528, indicating the cubic crystalline structure of $CuTi_2S_4$/rGO and pure $CuTi_2S_4$ and the space group of Fd-3m [27–30].

Further, the structure and formation of pure $CuTi_2S_4$ and rGO-combined $CuTi_2S_4$ composites were further examined by the Raman spectra, which are displayed in **Figure 1B.** From the Raman spectra of the $CuTi_2S_4$/rGO sample, the low-intensity D band, which was observed at 1348 cm^{-1}, corresponds to the disorder band (sp^3 hybridization), respectively. In contrast, the high-intensity G band appeared at 1592 cm^{-1}, indicating the presence of graphitic carbon (sp^2 hybridization) in samples [31–34]. More importantly, the strong band obtained at 1451 cm^{-1} confirms the presence of two metals with different coordination bonds [35]. Compared with pure $CuTi_2S_4$ samples, the composite $CuTi_2S_4$/rGO revealed a high intensity peak at 472 cm^{-1}, which is confirmed of the availability of Cu_2S in $CuTi_2S_4$/rGO [36].

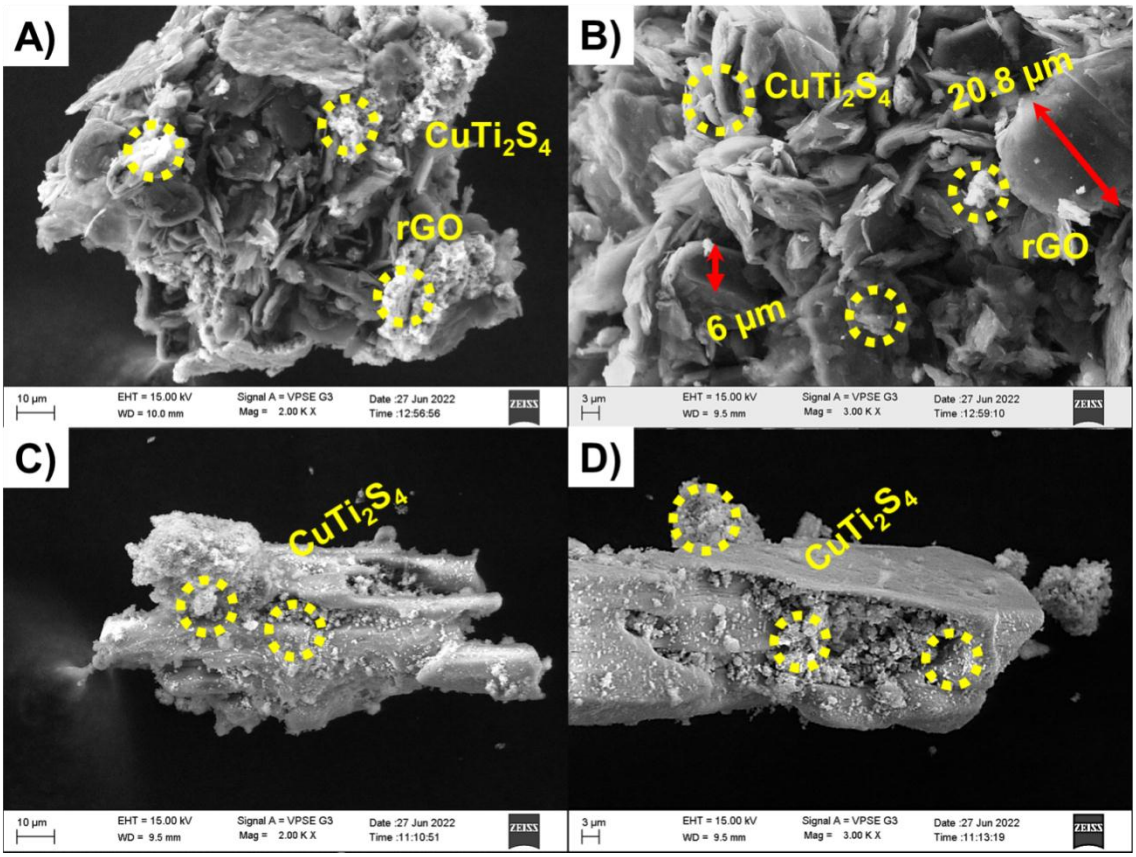

Figure 2. Low and high magnification FESEM images of the prepared the (A, B) $CuTi_2S_4$/rGO and pure (C, D) $CuTi_2S_4$ materials.

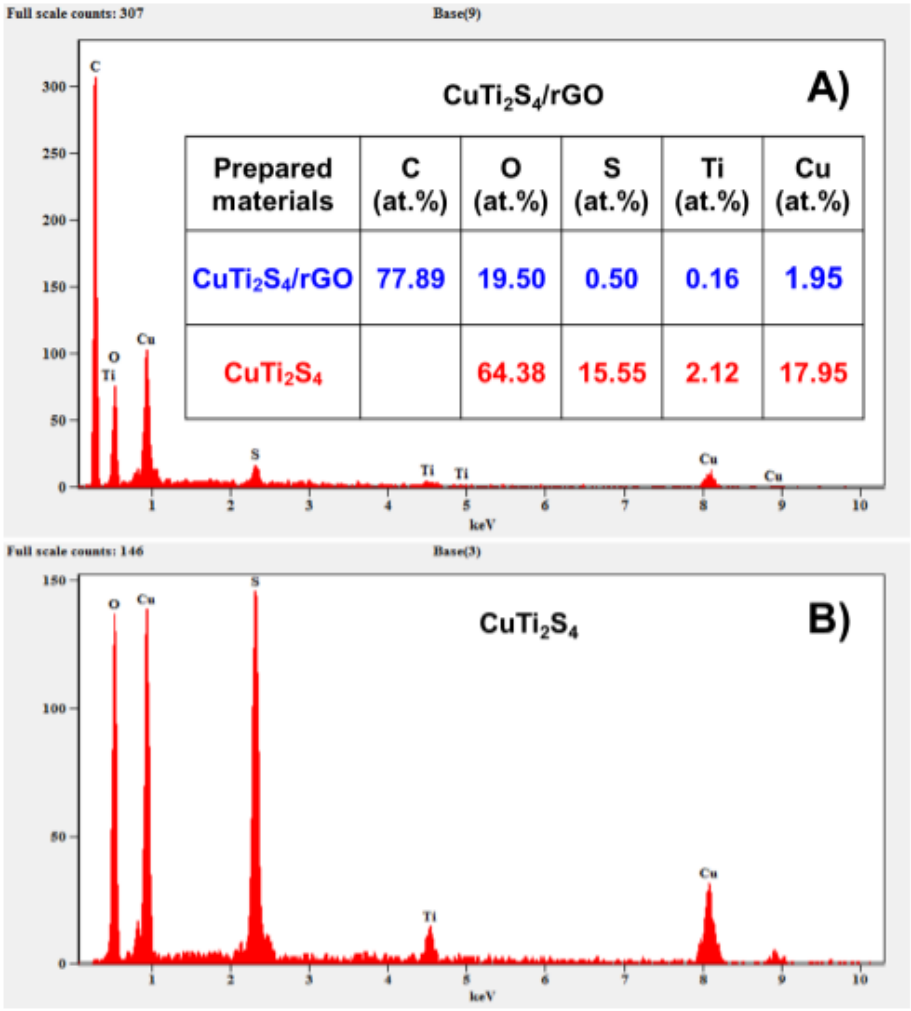

Prepared materials	C (at.%)	O (at.%)	S (at.%)	Ti (at.%)	Cu (at.%)
$CuTi_2S_4$/rGO	77.89	19.50	0.50	0.16	1.95
$CuTi_2S_4$		64.38	15.55	2.12	17.95

Figure 3. SEM EDX spectra of prepared (A) $CuTi_2S_4$/rGO, (B) $CuTi_2S_4$

In addition, the morphology of prepared $CuTi_2S_4$/rGO and $CuTi_2S_4$ pure samples was further examined by FESEM and HRTEM analyses. The FESEM images of $CuTi_2S_4$/rGO showed the ellipsoid-shaped morphology and its average diameter and thicknesses of 21 and 6 µm, respectively (**Figure 2**). These results pointed out that the $CuTi_2S_4$ particles are successfully dispersed on reduced graphene oxide sheets. Such a combination effectively contributed to the photocatalytic performance. Subsequently, the pure $CuTi_2S_4$ material showed an entirely different structure: a sponge with porous morphology due to the absence of rGO, which was further confirmed by EDX analysis [37]. The EDX analysis of both samples has been shown in **Figure 3**. where the Cu, Ti, and S are uniformly distributed and bound in rGO sheet-like structure. Their corresponding observed HRTEM images are shown in **Figure 4**. As shown in **Figure 4A-C**, cubic-shaped surfaces are occupied on the graphite sheet surface. Particularly **Figures 4B and 4C** presented high uniform cubic morphologies, and their sizes are labelled inside the figure. These results suggest that the $CuTi_2S_4$ effectively anchored over the graphene sheet structure develops the stable morphology and its respective SAED pattern given in **Figure 4D** [38,39]. The SAED pattern proposed that the highly uniform rings with various spots, imply the polycrystalline nature of $CuTi_2S_4$/rGO material [40].

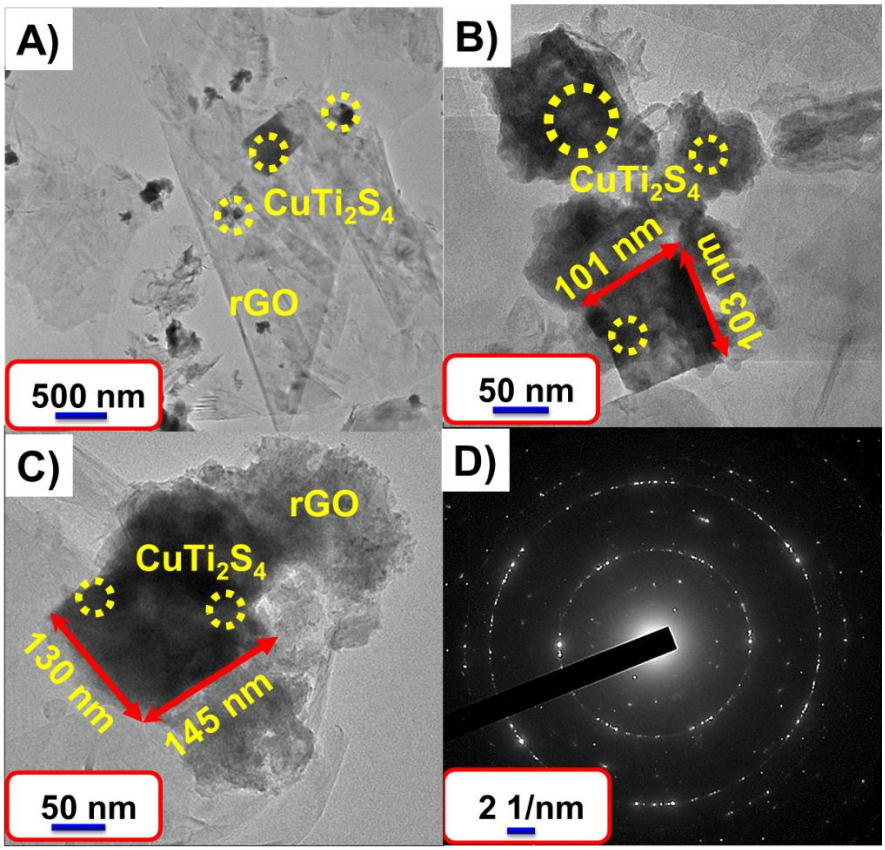

Figure 4. (A-C) Low and higher magnifications of **HR**TEM images of $CuTi_2S_4$/rGO and (D) their respected SAED pattern.

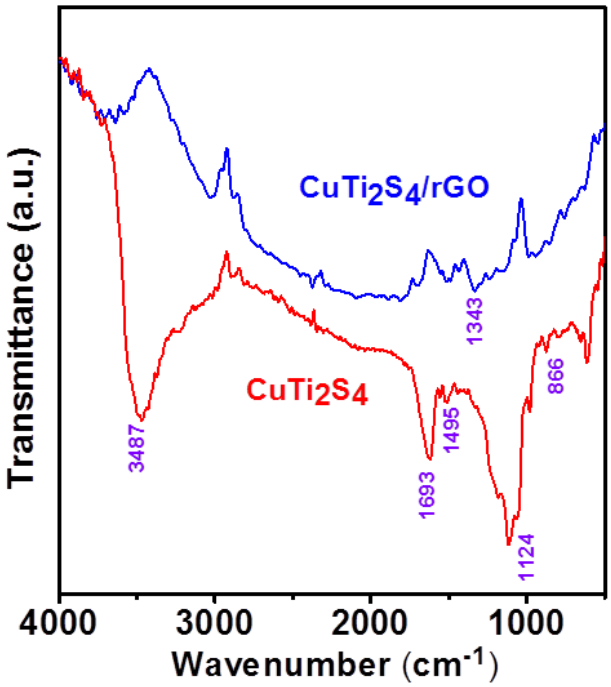

Figure 5. FTIR image of $CuTi_2S_4$/rGO and pure $CuTi_2S_4$ materials.

FT-IR spectra proves the bonding sites of synthesized materials, as presented in **Figure 5**. Remarkably, compared with the $CuTi_2S_4$ samples, in the $CuTi_2S_4$-doped $CuTi_2S_4$/rGO sample, most of the peaks were shifted and intensity was also altered due to the attaching effect of $CuTi_2S_4$ in reduced graphene oxide. In the case of $CuTi_2S_4$/rGO sample, a wide and strong peak at 3487 cm^{-1} attributed to the O-H stretching vibration of $CuTi_2S_4$ samples [41–45]. The $CuTi_2S_4$/rGO sample showed low intensity peaks at 1693 and 1490 cm^{-1}, which confirmed the presence of carbonyl compounds and C=C in the graphene oxide sample [41]. In addition, the low-intensity peak appeared at 1343 cm^{-1}, indicating the C-OH groups of $CuTi_2S_4$/rGO. This peak disappeared in the $CuTi_2S_4$ sample. It is one piece of evidence for $CuTi_2S_4$ effectively bound to the rGO and the formation of $CuTi_2S_4$/rGO. The other peak observed at 1124 cm^{-1} was attributed to C-O in the sample. The dual metals are combined in the rGO, which is supported by the peak at 866 cm^{-1}, which relates to the M-OH vibration of $CuTi_2S_4$/rGO composite [46]. These may significantly influence the photocatalytic activity.

3.2 Evaluation of photocatalytic activity

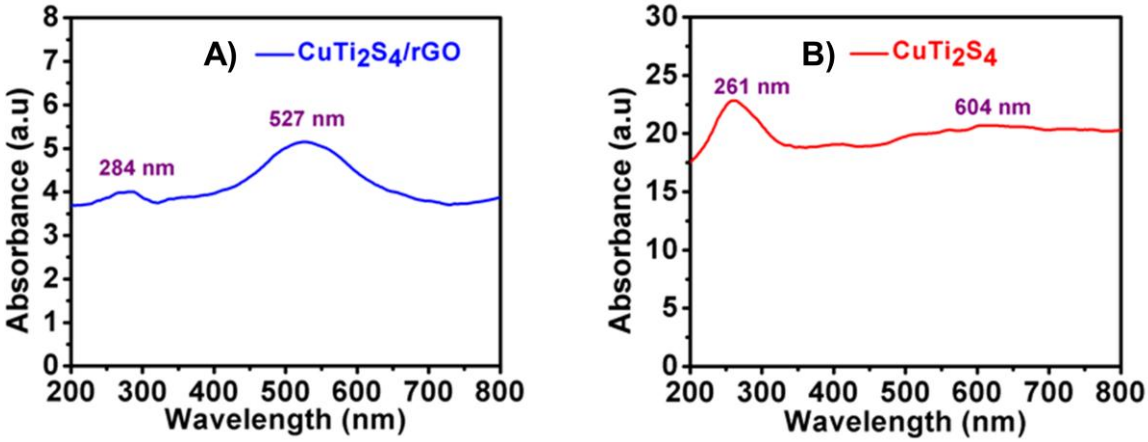

Figure 6. UV-Vis diffuse reflectance spectra of (A) $CuTi_2S_4$/rGO and (B) pure $CuTi_2S_4$ materials.

The optical properties of the $CuTi_2S_4$/rGO composite and pure materials were revealed by DRS. UV-Vis diffuse reflectance spectra can be employed to investigate the absorption edge information and the width of the forbidden band of prepared materials, as presented in **Figure 6.** It is noted from the results that the enhanced absorbance of the visible light region has been observed in rGO-introduced $CuTi_2S_4$/rGO than the pure $CuTi_2S_4$ material. This may be attributed to the incorporation of rGO in the $CuTi_2S_4$ sample, which in turn influences the optical properties of visible light absorption. Their corresponding bang gap spectra are presented in **Figure 7**, which is derived from the Tauc plot of UV-Vis spectra. The calculated band gap values of $CuTi_2S_4$/rGO and $CuTi_2S_4$ are 1.80 and 2.1 eV, respectively, which facilitate better photocatalytic activity. These results are one of the evidence for a considerable alteration in the photocatalytic activity. These values are in good agreement with previous reports [16,22,26,47,48].

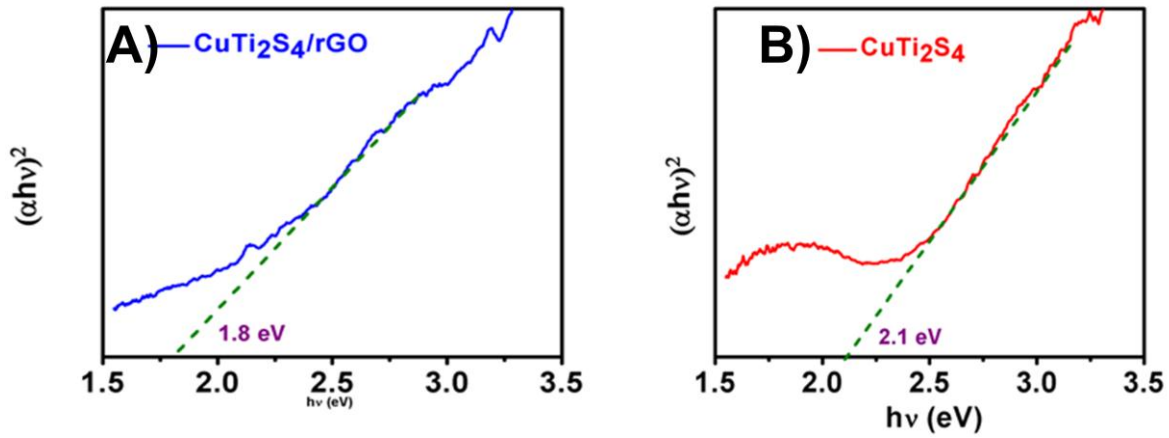

Figure 7. Band gap spectra of (A) $CuTi_2S_4$/rGO and pure (B) $CuTi_2S_4$ materials.

3.3 Photodegradability of reactive black-5 (RB-5)

The photocatalytic activities of prepared materials of rGO, $CuTi_2S_4$, and $CuTi_2S_4$/rGO composites were studied by degradation of reactive black-5 under solar light radiation. Here, the aromatic compound of RB-5 has highly effective candidates for light absorption in the UV-Visible region; thereby we have selected this material for the analysis. The resulted time profiles of C/Co are given in **Figure 8A**, where C is the concentration of RB-5 with irradiation time and Co is the concentration of adsorption or desorption equilibrium before the radiation [49,50].

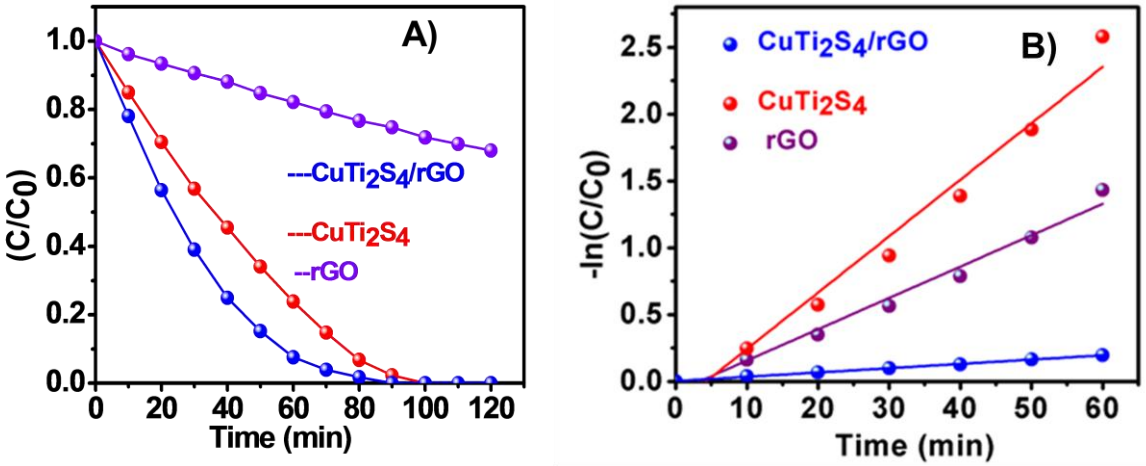

Figure 8. Photocatalytic activity of $CuTi_2S_4$/rGO, pure $CuTi_2S_4$ and rGO materials.

Figure 8A represents the improved photocatalytic activity shown in $CuTi_2S_4$/rGO compared with pure materials owing to the assessment of rGO and $CuTi_2S_4$. After 60 min, the solar light illumination of $CuTi_2S_4$/rGO with RB-5 degrades by only 20%. Overall, it showed a growth rate of 98%, indicating higher performance. In the case of pure $CuTi_2S_4$ and rGO exhibited 80 and 85% photocatalytic activity which are significantly lower than $CuTi_2S_4$/rGO composite. It is interesting to note that $CuTi_2S_4$/rGO demonstrated remarkable photo efficiency. This superior performance can be attributed to the following reasons such as the presence of the rGO effect, which could involve the transition of electrons to the $CuTi_2S_4$/rGO surface and lead to inhibition of the photogeneration charge recombination. Hence, the presence of rGO is significantly involved in the transition of valance band to conduction band electrons, which leads to the formation of new levels of energy via E_g of $CuTi_2S_4$. These

reduce the required energy for this transfer process [22,51].

In addition, above mentioned graphs showed good fitting, indicating first-order kinetics (**Figure 8B**). It is worth mentioning that conduction band electrons can be converted into adsorbed oxygen molecules to develop superoxide anions. Consequently, it can be transformed to OH* and promote the degradation of reactive black-5.

3.4 The reusability analysis of $CuTi_2S_4$/rGO composites

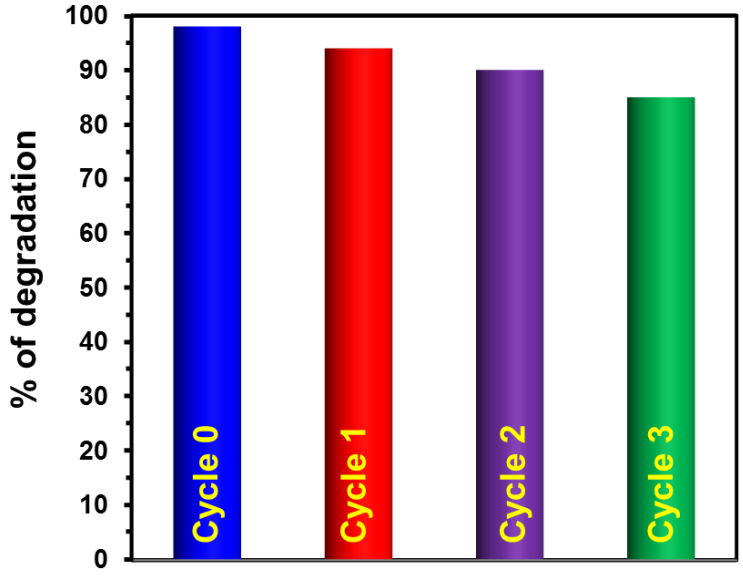

Figure 9. Reusability analysis of $CuTi_2S_4$/rGO materials with various cycles.

Further, we performed the photocatalytic reusability analysis of the best $CuTi_2S_4$/rGO composite for 0 to 3 cycles. During this experiment, the RB-5 solutions were replaced every 120 min and the degradation percentages were measured, as demonstrated in **Figure 9**. Hence, after every cycle, the $CuTi_2S_4$/rGO composite exhibited degradation rates for RB-5 of 98 (0 cycle), 94 (1 cycle), 90 (2 cycles) and 85% (3 cycles). It is worth noting that the degradation efficiency of the $CuTi_2S_4$/rGO composite gradually decreases with respect to cycles. Such an observation is recommended that due to the accumulation of intermediates during the degradation of RB-5 dye [52].

Proposed Mechanism

Based on UV-Vis DRS results the following mechanism was proposed. The mechanism has been presented in **Figure 10**.

$$CuTi_2S_4/rGO + h\nu \longrightarrow h^+ + e^-$$

In the visible light irradiation on $CuTi_2S_4$/rGO composite material, the electrons are excited in the valance band to conduction band to generate the h^+ in the valance band. In this case, the produced electrons are collected and transported by rGO. This leads to a significant separation of the electron hole pair, which subsequently boosts the charge carrier's lifetime. Then the photogenerated electrons have been reduced by the adsorbed O_2 on rGO to produce $\cdot HO_2$ species along with $\cdot O_2$- or OH radicals and their reactions are

$$\mathbf{e^- + O_2 \longrightarrow O_2^-}$$
$$\mathbf{\cdot O_2^- + H_2O \longrightarrow HO_2 + OH^-}$$
$$\mathbf{2\ \cdot HO_2 \longrightarrow H_2O_2 + O_2}$$
$$\mathbf{2\ \cdot HO_2 \longrightarrow H_2O_2 + O_2}$$
$$\mathbf{H_2O_2 + e^- \longrightarrow OH + OH^-}$$

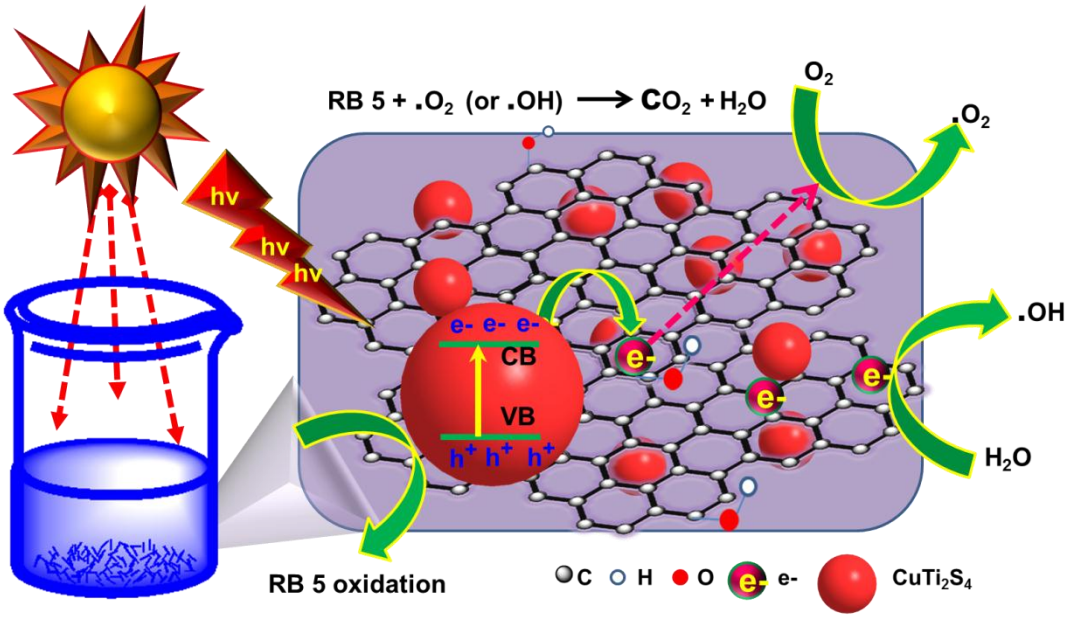

Figure 10. Proposed mechanism for the degradation of RB-5 over the $CuTi_2S_4$/rGO under visible light irradiation.

Then the RB-5 dye molecules can be degraded by the radicals $\cdot O_2^-$ and $\cdot OH$ to CO_2 and H_2O, and other products. In parallel, the photogenerated h^+ effectively react with the OH^- to produce OH. Consequently, it oxidises the absorbed RB-5 on the surface. Hence, RB-5 can be effectively degraded under visible light irradiation and improving performance stability and photocatalytic activity.

$$h^+ + H_2O \longrightarrow OH + H^+$$
$$\cdot O_2^-, \cdot OH + RB\text{-}5 \longrightarrow CO_2 + H_2O$$

4. Conclusions

In summary, we have successfully developed bimetallic copper, titanium, and sulfide ($CuTi_2S_4$) composite anchored over a reduced graphene oxide material through an effective hydrothermal treatment. The highly active $CuTi_2S_4$/rGO material was derived from copper nitrate, tetraethoxy titanium, and metallic sulfur precursors and the resulted materials were tested for photocatalytic performance with the help of the reactive black-5 dye. Compared with pure $CuTi_2S_4$ material, the reduced graphene oxide-combined $CuTi_2S_4$ material greatly influences the morphology and elemental contents of Cu, Ti, and S, which alter the photocatalytic performance. Remarkably, $CuTi_2S_4$/rGO demonstrated a notable performance compared to that of others. The uniform linkages of Cu, Ti, and S contents with the rGO significantly improved the absorption and desorption activity and the excellent charge carrier capability. Also, the synergistic effect between $CuTi_2S_4$ and rGO played a significant role in improving performance towards the degradation of RB-5 dye.

Author Statement

Priya Perumal: Conceptualization, Methodology, Data curation, Writing –editing original draft.

Lakshmi mahadevan: Conceptualization, supervision, review & editing.

Conflict of interest

The authors declare no conflict of interest for this work.

Disclosure statement

The authors declare no conflict of interest for this work.

5. References

[1] Z. Kalaycıoğlu, B. Özuğur Uysal, Ö. Pekcan, F.B. Erim, Efficient Photocatalytic Degradation of Methylene Blue Dye from Aqueous Solution with Cerium Oxide Nanoparticles and Graphene Oxide-

Doped Polyacrylamide, ACS Omega. 8 (2023) 13004–13015. https://doi.org/10.1021/acsomega.3c00198.

[2] L.G. Trung, M.K. Nguyen, T.D. Hang Nguyen, V.A. Tran, J.S. Gwag, N.T. Tran, Highly efficient degradation of reactive black KN-B dye by ultraviolet light responsive ZIF-8 photocatalysts with different morphologies, RSC Adv. 13 (2023) 5908–5924. https://doi.org/10.1039/D2RA08312D.

[3] G. Yi, "Cobalt Doped TiO2/rGO Nanocomposites as Highly Efficient Photocatalyst for Water Purification," Biomed. J. Sci. Tech. Res. 37 (2021) 29249–29257. https://doi.org/10.26717/BJSTR.2021.37.005972.

[4] A. Muthukrishnaraj, S.A. Al-Zahrani, A. Al Otaibi, S.S. Kalaivani, A. Manikandan, N. Balasubramanian, A.L. Bilgrami, M.A.R. Ahamed, A. Khan, A.M. Asiri, N. Balasubramanian, Enhanced Photocatalytic Activity of Cu2O Cabbage/RGO Nanocomposites under Visible Light Irradiation, Polymers (Basel). 13 (2021) 1712. https://doi.org/10.3390/polym13111712.

[5] S. Velusamy, A. Roy, S. Sundaram, T. Kumar Mallick, A Review on Heavy Metal Ions and Containing Dyes Removal Through Graphene Oxide-Based Adsorption Strategies for Textile Wastewater Treatment, Chem. Rec. 21 (2021) 1570–1610. https://doi.org/10.1002/tcr.202000153.

[6] A. Saravanan, P. Senthil Kumar, S. Jeevanantham, S. Karishma, B. Tajsabreen, P.R. Yaashikaa, B. Reshma, Effective water/wastewater treatment methodologies for toxic pollutants removal: Processes and applications towards sustainable development, Chemosphere. 280 (2021) 130595. https://doi.org/10.1016/j.chemosphere.2021.130595.

[7] V. Duraisamy, V. Sudha, V. Dharuman, S.M. Senthil Kumar, Highly Efficient Electrochemical Sensing of Acetaminophen by Cobalt Oxide-Embedded Nitrogen-Doped Hollow Carbon Spheres, ACS Biomater. Sci. Eng. 9 (2023) 1682–1693. https://doi.org/10.1021/acsbiomaterials.2c01248.

[8] K. Li, R. Cheng, Q. Xue, T. Zhao, F. Wang, C. Fu, Construction of a Co/MnO Mott–Schottky Heterostructure to Achieve Interfacial Synergy in the Oxygen Reduction Reaction for Aluminum–Air Batteries, ACS Appl. Mater. Interfaces. 15 (2023) 9150–9159. https://doi.org/10.1021/acsami.2c13871.

[9] N. Kumar, K. Naveen, M. Kumar, T.C. Nagaiah, R. Sakla, A. Ghosh, V. Siruguri, S. Sadhukhan, S. Kanungo, A.K. Paul, Multifunctionality Exploration of Ca 2 FeRuO 6 : An Efficient Trifunctional Electrocatalyst toward OER/ORR/HER and Photocatalyst for Water Splitting, ACS Appl. Energy Mater. 4 (2021) 1323–1334. https://doi.org/10.1021/acsaem.0c02579.

[10] Y. Liu, X. Wu, Recent Advances of Transition Metal Chalcogenides as Cathode Materials for Aqueous Zinc-Ion Batteries, Nanomaterials. 12 (2022) 1–16. https://doi.org/10.3390/nano12193298.

[11] H. Kumari, Sonia, Suman, R. Ranga, S. Chahal, S. Devi, S. Sharma, S. Kumar, P. Kumar, S. Kumar, A. Kumar, R. Parmar, A Review on Photocatalysis Used For Wastewater Treatment: Dye Degradation, Water, Air, Soil Pollut. 234 (2023) 349. https://doi.org/10.1007/s11270-023-06359-9.

[12] M. Saranya, C. Santhosh, S.P. Augustine, A.N. Grace, Synthesis and characterisation of CuS nanomaterials using hydrothermal route, J. Exp. Nanosci. 9 (2014) 329–336. https://doi.org/10.1080/17458080.2012.661471.

[13] K. Krishnamoorthy, G. Kumar Veerasubramani, A.N. Rao, S. Jae Kim, One-pot hydrothermal synthesis,

characterization and electrochemical properties of CuS nanoparticles towards supercapacitor applications, Mater. Res. Express. 1 (2014) 035006. https://doi.org/10.1088/2053-1591/1/3/035006.

[14] M. Saranya, A. Nirmala Grace, Hydrothermal Synthesis of CuS Nanostructures with Different Morphology, J. Nano Res. 18–19 (2012) 43–51. https://doi.org/10.4028/www.scientific.net/JNanoR.18-19.43.

[15] G. Ramalingam, R. Vignesh, C. Ragupathi, C.M. Magdalane, K. Kaviyarasu, J. Kennedy, Electrical and chemical stability of CuS nanofluids for conductivity of water soluble based nanocomposites, Surfaces and Interfaces. 19 (2020) 100475. https://doi.org/10.1016/j.surfin.2020.100475.

[16] B. Pejjai, M. Reddivari, T.R.R. Kotte, Phase controllable synthesis of CuS nanoparticles by chemical co-precipitation method: Effect of copper precursors on the properties of CuS, Mater. Chem. Phys. 239 (2020) 122030. https://doi.org/10.1016/j.matchemphys.2019.122030.

[17] P. Arumugam, P. Sengodan, N. Duraisamy, R. Rajendran, V. Vasudevan, An effective strategy to enhance the photocatalytic performance by forming NiS/rGO heterojunction nanocomposites, Ionics (Kiel). 26 (2020) 4201–4212. https://doi.org/10.1007/s11581-020-03564-y.

[18] S. Dutta, S. Chatterjee, I. Mukherjee, R. Saha, B.P. Singh, Fabrication of ZnS Hollow Spheres and RGO-ZnS Nanocomposite Using Cysteamine as Novel Sulfur Source: Photocatalytic Performance on Industrial Dyes and Effluent, Ind. Eng. Chem. Res. 56 (2017) 4768–4778. https://doi.org/10.1021/acs.iecr.7b00107.

[19] X.-S. Hu, Y. Shen, Y.-T. Zhang, J.-J. Nie, Preparation of flower-like CuS/reduced graphene oxide(RGO) photocatalysts for enhanced photocatalytic activity, J. Phys. Chem. Solids. 103 (2017) 201–208. https://doi.org/10.1016/j.jpcs.2016.12.021.

[20] J. Shi, X. Zhou, Y. Liu, Q. Su, J. Zhang, G. Du, Sonochemical synthesis of CuS/reduced graphene oxide nanocomposites with enhanced absorption and photocatalytic performance, Mater. Lett. 126 (2014) 220–223. https://doi.org/10.1016/j.matlet.2014.04.051.

[21] Y. Cherifi, A. Barras, A. Addad, B. Ouddane, P. Roussel, A. Chaouchi, S. Szunerits, R. Boukherroub, Simultaneous photocatalytic Cr(VI) reduction and phenol degradation over copper sulphide-reduced graphene oxide nanocomposite under visible light irradiation: Performance and reaction mechanism, Chemosphere. 268 (2021) 128798. https://doi.org/10.1016/j.chemosphere.2020.128798.

[22] S. Vadivel, B. Paul, A. Habibi-Yangjeh, D. Maruthamani, M. Kumaravel, T. Maiyalagan, One-pot hydrothermal synthesis of CuCo2S4/RGO nanocomposites for visible-light photocatalytic applications, J. Phys. Chem. Solids. 123 (2018) 242–253. https://doi.org/10.1016/j.jpcs.2018.08.011.

[23] S. Yao, L. Xu, Q. Gao, X. Wang, N. Kong, W. Li, J. Wang, G. Li, X. Pu, Enhanced photocatalytic degradation of Rhodamine B by reduced graphene oxides wrapped-Cu2SnS3flower-like architectures, J. Alloys Compd. 704 (2017) 469–477. https://doi.org/10.1016/j.jallcom.2017.02.069.

[24] Z. Lei, W. You, M. Liu, G. Zhou, T. Takata, M. Hara, K. Domen, C. Li, Photocatalytic water reduction under visible light on a novel ZnIn2S4 catalyst synthesized by hydrothermal method, Chem. Commun. 3 (2003) 2142–2143. https://doi.org/10.1039/b306813g.

[25] J. Ding, W. Yan, S. Sun, J. Bao, C. Gao, Hydrothermal synthesis of CaIn2S4-reduced graphene oxide nanocomposites with increased photocatalytic performance, ACS Appl. Mater. Interfaces. 6 (2014) 12877–12884. https://doi.org/10.1021/am5028296.

[26] G. Gnanamoorthy, P. Priya, D. Ali, M. Lakshmi, V.K. Yadav, R. Varghese, A new CuZr2S4/rGO and their reduced graphene oxide nanocomposities enhanced photocatalytic and antimicrobial activities, Chem. Phys. Lett. 781 (2021) 139011. https://doi.org/10.1016/j.cplett.2021.139011.

[27] N. Matsumoto, T. Hagino, K. Taniguchi, S. Chikazawa, S. Nagata, Electrical and magnetic properties of CuTi2S4 and CuZr2S4, Phys. B Condens. Matter. 284–288 (2000) 1978–1979. https://doi.org/10.1016/S0921-4526(99)02946-4.

[28] V. Duraisamy, N. Arumugam, A.I. Almansour, Y. Wang, T.X. Liu, S.M.S. Kumar, In situ decoration of Co3O4 on N-doped hollow carbon sphere as an effective bifunctional oxygen electrocatalyst for oxygen evolution and oxygen reduction reactions, Colloids Surfaces A Physicochem. Eng. Asp. 656 (2023) 130347. https://doi.org/10.1016/j.colsurfa.2022.130347.

[29] S. Roy Chowdhury, T. Maiyalagan, CuCo2S4@B,N-Doped Reduced Graphene Oxide Hybrid as a Bifunctional Electrocatalyst for Oxygen Reduction and Evolution Reactions, ACS Omega. 7 (2022) 19183–19192. https://doi.org/10.1021/acsomega.2c00183.

[30] N. Soheilnia, K.M. Kleinke, E. Dashjav, H.L. Cuthbert, J.E. Greedan, H. Kleinke, Crystal structure and physical properties of a new CuTi2S 4 modification in comparison to the thiospinel, Inorg. Chem. 43 (2004) 6473–6478. https://doi.org/10.1021/ic0495113.

[31] M. Mahanthappa, V. Duraisamy, P. Arumugam, S.M. Senthil Kumar, Simultaneous Determination of Ascorbic Acid, Dopamine, Uric Acid, and Acetaminophen on N, P-Doped Hollow Mesoporous Carbon Nanospheres, ACS Appl. Nano Mater. 5 (2022) 18417–18426. https://doi.org/10.1021/acsanm.2c04170.

[32] N. Sivaraman, V. Duraisamy, S.M. Senthil Kumar, R. Thangamuthu, N, S dual doped mesoporous carbon assisted simultaneous electrochemical assay of emerging water contaminant hydroquinone and catechol, Chemosphere. 307 (2022) 135771. https://doi.org/10.1016/j.chemosphere.2022.135771.

[33] V. Duraisamy, S.M. Senthil Kumar, N and P dual heteroatom doped mesoporous hollow carbon as an efficient oxygen reduction reaction catalyst in alkaline electrolyte, Int. J. Hydrogen Energy. 47 (2022) 17992–18006. https://doi.org/10.1016/j.ijhydene.2022.03.284.

[34] V. Duraisamy, S. Venkateshwaran, R. Thangamuthu, S.M. Senthil Kumar, Hard template derived N, S dual heteroatom doped ordered mesoporous carbon as an efficient electrocatalyst for oxygen reduction reaction, Int. J. Hydrogen Energy. 47 (2022) 40327–40339. https://doi.org/10.1016/j.ijhydene.2022.03.250.

[35] K.I. Hadjiivanov, D.A. Panayotov, M.Y. Mihaylov, E.Z. Ivanova, K.K. Chakarova, S.M. Andonova, N.L. Drenchev, Power of Infrared and Raman Spectroscopies to Characterize Metal-Organic Frameworks and Investigate Their Interaction with Guest Molecules, Chem. Rev. 121 (2021) 1286–1424. https://doi.org/10.1021/acs.chemrev.0c00487.

[36] X. Shuai, W. Shen, Z. Hou, S. Ke, C. Xu, C. Jiang, A versatile chemical conversion synthesis of Cu2S nanotubes and the photovoltaic

activities for dye-sensitized solar cell, Nanoscale Res. Lett. 9 (2014) 513. https://doi.org/10.1186/1556-276X-9-513.

[37] F. Wang, J. Zheng, J. Ma, K. Zhou, Q. Wang, One-step facile route to glucose/copper cobalt sulfide nanorod for high-performance asymmetric supercapacitors, J. Nanoparticle Res. 21 (2019) 189. https://doi.org/10.1007/s11051-019-4614-2.

[38] D. Chen, L. Zou, S. Li, F. Zheng, Nanospherical like reduced graphene oxide decorated TiO 2 nanoparticles: An advanced catalyst for the hydrogen evolution reaction, Sci. Rep. 6 (2016). https://doi.org/10.1038/srep20335.

[39] Z. Fang, L. Long, S. Hao, Y. Song, T. Qiang, B. Geng, Mesocrystal precursor transformation strategy for synthesizing ordered hierarchical hollow TiO2 nanobricks with enhanced photocatalytic property, CrystEngComm. 16 (2014) 2061–2069. https://doi.org/10.1039/c3ce41970c.

[40] G. Žerjav, M.S. Arshad, P. Djinović, I. Junkar, J. Kovač, J. Zavašnik, A. Pintar, Improved electron-hole separation and migration in anatase TiO2 nanorod/reduced graphene oxide composites and their influence on photocatalytic performance, Nanoscale. 9 (2017) 4578–4592. https://doi.org/10.1039/c7nr00704c.

[41] P. Singh, P. Nath, R.K. Arun, S. Mandal, N. Chanda, Novel synthesis of a mixed Cu/CuO–reduced graphene oxide nanocomposite with enhanced peroxidase-like catalytic activity for easy detection of glutathione in solution and using a paper strip, RSC Adv. 6 (2016) 92729–92738. https://doi.org/10.1039/C6RA20882G.

[42] P. Naveenkumar, G. Paruthimal Kalaignan, Fabrication of core-shell like hybrids of CuCo2S4@NiCo(OH)2 nanosheets for supercapacitor applications, Compos. Part B Eng. 173 (2019) 106864. https://doi.org/10.1016/j.compositesb.2019.05.075.

[43] V. Duraisamy, R. Krishnan, S.M.S. Kumar, Architecture of large surface area N-doped mesoporous carbon sheets as sustainable electrocatalyst for oxygen reduction reaction in alkaline electrolyte, Mater. Res. Bull. 149 (2022) 111729. https://doi.org/10.1016/j.materresbull.2022.111729.

[44] V. Duraisamy, R. Krishnan, S.M.S. Kumar, Architecture of large surface area N-doped mesoporous carbon sheets as sustainable electrocatalyst for oxygen reduction reaction in alkaline electrolyte, Mater. Res. Bull. 149 (2022) 111729. https://doi.org/10.1016/j.materresbull.2022.111729.

[45] V. Duraisamy, S.M.S. Kumar, Study of the Secondary Heteroatoms Doping on Nitrogen-Doped Carbon and Their Oxygen Reduction Reaction Performance Evaluation, ChemistrySelect. 6 (2021) 11887–11899. https://doi.org/10.1002/slct.202103506.

[46] S. Sagadevan, J.A. Lett, G.K. Weldegebrieal, S. Garg, W. Oh, N.A. Hamizi, M.R. Johan, Enhanced Photocatalytic Activity of rGO-CuO Nanocomposites for the Degradation of Organic Pollutants, Catalysts. 11 (2021) 1008. https://doi.org/10.3390/catal11081008.

[47] J. Nai, Y. Lu, X.Y. Yu, Formation of Ti-Fe mixed sulfide nanoboxes for enhanced electrocatalytic oxygen evolution, J. Mater. Chem. A. 6 (2018) 21891–21895. https://doi.org/10.1039/c8ta02334d.

[48] J. Sun, C. Wang, T. Shen, H. Song, D. Li, R. Zhao, X. Wang, Engineering the Dimensional Interface of BiVO4-2D Reduced Graphene Oxide (RGO) Nanocomposite for Enhanced Visible Light Photocatalytic Performance, Nanomaterials. 9 (2019) 907. https://doi.org/10.3390/nano9060907.

[49] H. Nassehinia, H. Rahmani, K. Rahmani, A. Rahmani, Solar photocatalytic degradation of Reactive Black 5: by-products, bio-toxicity, and kinetic study, Desalin. WATER Treat. 206 (2020) 385–395.

https://doi.org/10.5004/dwt.2020.26269.

[50] M.P. da Silva, A.C.A. de Souza, L.E. de Lima Ferreira, L.M. Pereira Neto, B.F. Nascimento, C.M.B. de Araújo, T.J.M. Fraga, M.A. da Motta Sobrinho, M.G. Ghislandi, Photodegradation of Reactive Black 5 and raw textile wastewater by heterogeneous photo-Fenton reaction using amino-Fe3O4-functionalized graphene oxide as nanocatalyst, Environ. Adv. 4 (2021) 100064. https://doi.org/10.1016/j.envadv.2021.100064.

[51] H. Sun, O.A. Zelekew, X. Chen, Y. Guo, D.-H. Kuo, Q. Lu, J. Lin, A noble bimetal oxysulfide Cu V OS catalyst for highly efficient catalytic reduction of 4-nitrophenol and organic dyes, RSC Adv. 9 (2019) 31828–31839. https://doi.org/10.1039/C9RA05172D.

[52] M. Pudukudy, Q. Jia, Y. Dong, Z. Yue, S. Shan, Magnetically separable and reusable rGO/Fe 3 O 4 nanocomposites for the selective liquid phase oxidation of cyclohexene to 1,2-cyclohexane diol, RSC Adv. 9 (2019) 32517–32534. https://doi.org/10.1039/C9RA04685B.